International Journal of Power Electronics and Drive System (IJPEDS)
Vol. 17, No. 1, March 2026, pp. 602~616
ISSN: 2088-8694, DOI: 10.11591/ijpeds.v17.i1.pp602-616

A new boost LED driver

Dzhunusbekov Erlan[1], Orazbayev Sagi[2]
[1]Laboratory of Perspective Developments in Electronics, JSC "Kazakh-British Technical University", Almaty, Kazakhstan
[2]Al-Farabi Kazakh National University, Almaty, Kazakhstan

Article Info

Article history:

Received Jun 10, 2025
Revised Feb 5, 2026
Accepted Feb 15, 2026

Keywords:

Boost LED driver
Direct AC LED module
High voltage LED driver
Hybrid LED driver
LED street lighting
Reliability

ABSTRACT

Reducing the cost, increasing efficiency, and improving the reliability of LED drivers are critical due to the widespread adoption of LED lighting. This paper presents a research study on a novel boost LED driver designed to minimize voltage pulsations across power switches, thereby reducing dynamic losses in all power components. A small number of Schottky diodes were used to reduce conduction losses. To reduce switching losses in semiconductors, a quasi-resonant switching (QRS) at zero current was implemented for driving transistors. The operating principle is analyzed using computer modeling and validated experimentally in critical conduction mode (CrCM). In the initial evaluation, one version of the proposed driver achieved a high efficiency of up to 98.7% at 120 W input power. Additionally, the size and value of the main inductor were significantly reduced. The proposed driver provides an efficient and scalable solution for high-power LED lighting. Lower dynamic losses and reduced impulse voltages create opportunities for integrating the control circuit and power switches into a single chip.

Corresponding Author:

Dzhunusbekov Erlan
Laboratory of Perspective Developments in Electronics, JSC "Kazakh-British Technical University"
Tole-bi Street, House 59, Almaty 050060, Kazakhstan
Email: erlan555dj@yahoo.com

1. INTRODUCTION

The rapid adoption of LED lighting has transformed the industry, offering unparalleled energy efficiency, longevity, and environmental benefits. However, despite these advantages, the performance and cost-effectiveness of LED lighting systems remain constrained by the limitations of LED drivers. Advancements in LED driver technology are critically important due to the widespread application of lighting in various aspects of human life and industry. As LED chip prices continue to decline, the relative cost of LED drivers has become a dominant factor in the overall expense of lighting systems. While LED chips have lifespans exceeding 50,000 hours, conventional LED drivers often fail much sooner due to their complex circuitry [1]-[7]. There are proposals to eliminate electrolytic capacitors to improve reliability [8]-[14].

A notable trend in modern LED driver development is the integration of control and power circuits within a single semiconductor device [15], [16]. This approach aims to reduce costs, minimize the footprint on printed circuit boards, and enhance reliability. A significant trend has been the development of direct AC LED modules [16]-[21], which eliminate the need for traditional LED drivers. This approach dynamically adjusts LED arrays to match the alternating mains voltage using low-frequency switching synchronized with the grid. Direct AC LED modules offer a cost-effective and structurally simple solution, as they eliminate the need for high-speed power switches, transformers, inductors, and electrolytic capacitors with limited lifespans, and high-frequency filtering components. Their minimalistic design makes them well-suited for integration, and commercially available ICs have already been introduced to the market. However, a key

drawback of AC LED modules is the presence of linear current regulators, which lead to power losses and thermal dissipation issues. Currently, most commercially available solutions are designed for low-power applications, limiting their broader adoption in high-power lighting systems.

To enhance efficiency, a hybrid LED Driver has been proposed [22]-[25]. This design incorporates a dynamically reconfigurable load of LED strings, similar to direct AC LED modules, aligning them with the instantaneous mains voltage. However, to compensate for the voltage difference between the LED string voltage and the varying mains voltage, a small inductor and an optimized switching algorithm for the configuration MOSFETs are introduced. The switching MOSFETs, in conjunction with the inductor, regulate the overall circuit impedance, thereby controlling the input current. This auxiliary converter handles only a fraction of the total output power and operates with low pulse voltage across the main inductor and power switches. As a result, the hybrid LED driver offers potential for circuit integration by combining control logic and power MOSFETs within a single semiconductor device. In studies [22]-[24], slow LED strings are controlled directly by transistors, which poses problems with hard switching, which limits efficiency, EMI performance, and scalability to high-power and high-voltage applications. To eliminate hard switching of transistors, the use of fast diodes connected in series with transistors has been proposed [25]. Although the conduction losses in the diodes reported in [25] are limited to a single conduction diode at any given time, the losses are nevertheless high due to the fact that high-voltage diodes must be used for the 400 V output LED load. Efficiency improvements for high-power applications typically require subdividing the LED load into many small strings, which increases circuit complexity and the number of power devices.

As a result, there remains a lack of LED driver solutions that simultaneously support high power operation, high efficiency, and compact, integration-friendly designs while maintaining low cost and high reliability. This paper addresses this gap by proposing a boost-type hybrid LED driver topology. In the proposed solution, a limited number of Schottky diodes are employed to reduce conduction losses, while zero-current quasi-resonant switching (QRS) is implemented to further minimize switching losses.

Even a marginal improvement in efficiency is of critical importance, given the accelerating adoption of LED lighting across applications that were previously unfeasible. Such advancements translate into substantial energy and cost savings on a global scale.

2. THE PROPOSED METHOD

Two modified boost LED drivers were investigated, as shown in Figure 1. The drivers include dynamically switched LED strings, as well as Schottky diodes connected in series with the LED strings. Provided that the number of LED strings does not exceed three, the combined conduction losses of the Schottky diodes are less than the losses in the single diode of the conventional boost LED driver. Switching losses in Schottky diodes are kept low due to the QRS of the transistors operating in the CrCM.

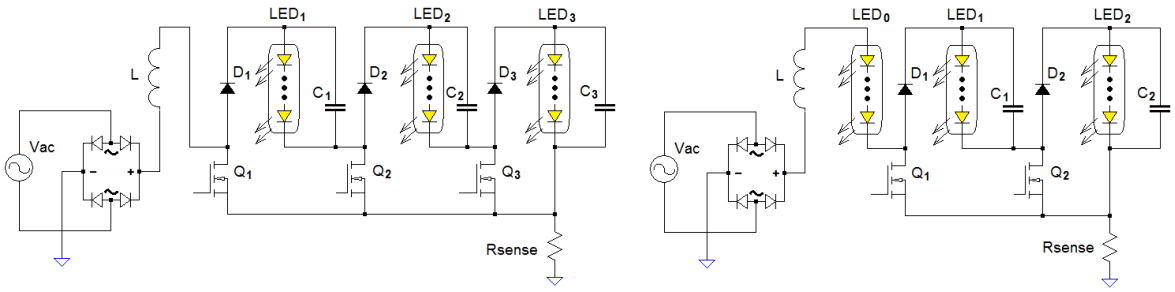

Figure 1. The proposed boost LED drivers: (a) first driver and (b) second driver

In this work, two proposed LED boost drivers were studied theoretically and experimentally. The driver topology shown in Figure 1(a) includes three active power transistors and three protective diodes and provides the best power factor. The highest efficiency, however, was achieved with the driver topology shown in Figure 1(b), which employs two active transistors and two protective diodes. The apparent circuit complexity in Figure 1 can be addressed by integrating the control circuitry with the power switches.

The following sections introduce the proposed topologies and analyze their operating principles. The theoretical study is limited to the investigation of a computer model. The hysteresis current control in continuous conduction mode (CCM) was considered for simplicity and generality. Subsequently, 200 W

experimental prototypes were developed and tested. A CrCM was implemented as a special case of the hysteresis control. A comparative analysis was conducted between the proposed drivers and a conventional boost driver with high-efficiency in an industry. Finally, key findings are discussed, and conclusions are presented.

2.1. The first proposed boost LED driver

First, the boost LED driver shown in Figure 1(a) is analyzed to demonstrate its feasibility and advantages. The operating principle of the proposed driver is similar to that of the hybrid LED driver described in [25], except that the protective diodes D_1-D_3 are not connected in series with the power transistors Q_1-Q_3 but are instead connected in series with the LED load segments LED_1-LED_3. The driver operation is divided into discrete operating stages, denoted as Stage(K), during which only one transistor Q_K is actively pulse-width modulated at any given time. The power transistors Q_1-Q_3 are proposed to switch according to the following switching procedure.

At a given instantaneous input voltage Vin, if the total forward voltage of the LEDs meets the condition $V_{LED0}+V_{LED1}+...+V_{LED(K-1)}<$ Vin $<V_{LED0}+V_{LED1}+...$ $...+V_{LED(K)}$, then pulse-width mode (PWM) regulation of Stage(K) is activated: transistors Q_1 to $Q_{(K-1)}$ remain in the cutoff state; transistors $Q_{(K+1)}$ to Q_3 are conducting, and only $Q_{(K)}$ actively regulates the input current. During the active Stage(K), when the transistor Q_K is in the ON-state, the inductor current increases according to (1); when the transistor Q_K is in the OFF-state, the inductor current decreases according to (2). In this manner, the input current is regulated within predefined limits.

$$\frac{dI_L}{dt} = \frac{Vin - V_{LED1} - \cdots - V_{LED(K-1)}}{L} \rightarrow \left|\frac{dI_L}{dt}\right| < \frac{V_{LED(K)}}{L} \quad (1)$$

$$\frac{dI_L}{dt} = -\frac{V_{LED1} + \cdots + V_{LED(K-1)} + V_{LED(K)} - Vin}{L} \rightarrow \left|\frac{dI_L}{dt}\right| < \frac{V_{LED(K)}}{L} \quad (2)$$

For the active transistor Q_K and diode D_K, the switching voltage amplitude matches the string voltage $V_{LED(K)}$. For the inductor L, the voltage amplitude remains lower than $V_{LED(K)}$, as shown in (1) and (2).

During Stage(K), as the input voltage Vin exceeds $V_{LED0}+V_{LED1}+...+V_{LED(K)}$, transistor Q_K switches OFF, and transistor Q_{K+1} begins PWM operation, transitioning the driver to Stage(K+1). Conversely, as Vin drops below $V_{LED0}+V_{LED1}+...+V_{LED(K-1)}$ during Stage(K), transistor Q_K switches ON, while Q_{K-1} takes over the switching operation, shifting the proposed driver into Stage(K−1).

In the work [22], to increase immunity to noise and for simplicity, it was proposed to make transitions between Stage(K+1), Stage(K), and Stage(K-1) based on the current signal and not on the input voltage level. In this work, the following current-control transition procedure is proposed. If during Stage(K) the inductor current exceeds the upper threshold while transistor Q_K is switched OFF, transistor Q_{K+1} initiates PWM operation from its initial ON state, thereby connecting the LED_{K+1} string to counteract further current rise. Thus, the driver enters Stage(K+1). In the opposite case, if the inductor current drops to the lower threshold while transistor Q_K is switched ON, transistor Q_{K-1} starts PWM operation from its initial OFF state. The LED_K string remains inactive to counteract the downward current trend. As a result, the proposed driver enters Stage(K−1).

A computer model was developed to simulate the first proposed driver shown in Figure 1(a), which includes three active transistors. In this configuration, the simulated circuit maintains pulsed switching operation even near zero input voltage, |Vin|≈0. Figure 2 illustrates the implementation of a hysteresis current control scheme. The simulation setup consists of the power train and the control circuit. The power train includes an AC input voltage source Vin, a diode bridge rectifier, the boost inductor L, and a segmented LED load consisting of strings LED_1-LED_3 controlled by three power transistors Q_1-Q_3. The control circuit implements hysteresis-based current regulation, operates in continuous conduction mode for generality, and achieves PFC through direct regulation of the inductor current while enabling dynamic reconfiguration of the LED strings. The constructed model control follows a conventional PFC architecture based on hysteresis control of the main inductor current. The operational amplifier U1 sets the upper and lower current thresholds I_high and I_low proportionally to the alternating input voltage. Comparators Comp_L and Comp_H continuously track the inductor current I_L to ensure it remains within the reference I_high and I_low to follow input voltage shape. The DEMUX block manages the transition between stages Stage(K)↔Stage(K+1) when needed. The principles of the DEMUX block stage transitions and the corresponding control algorithm are implemented exactly as described in [25]. If a transition is not needed, the DEMUX block propagates a PWM governing pulses from a flip-flop trigger to the active transistor Q_K without interference, while holding gates of transistors Q_1-Q_{K-1} at zero and keeping the gates of transistors Q_{k+1}-Q_3 at a high level. The input voltage is set to Vin = 230 Vrms with an input power of 136 W. For better visualization in simulation, the inductor L is

chosen as 10 mH to reduce the switching frequency and make the pulse switching traceable throughout the input phase cycle. The voltage drops of LED strings are set as V_{LED1} = 136 V, V_{LED2} = 133 V, and V_{LED3} = 132 V to match experimental setup values. The total LED voltage drop is 401 V.

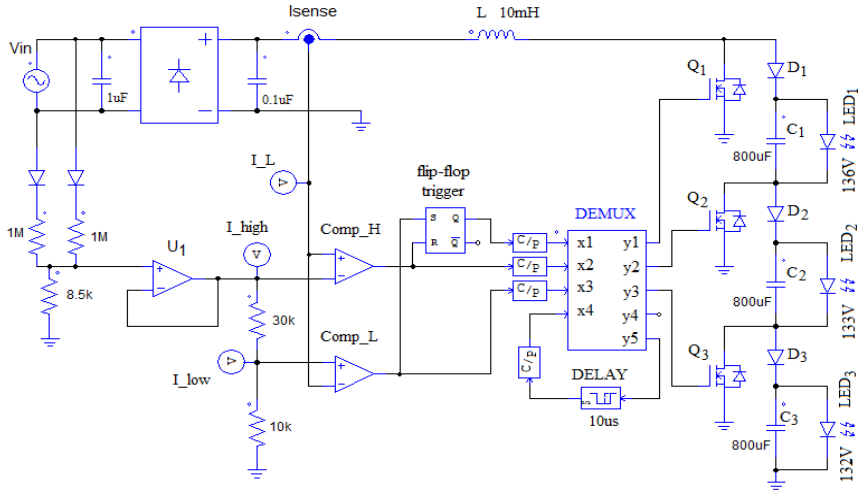

Figure 2. Computer simulation model of the first proposed boost LED driver

Figure 3 presents the steady-state waveforms obtained from the simulation for a single half-period of the input voltage. The design demonstrates reduced voltage swings across inductor L, power transistors Q_1-Q_3, and rectifier diodes D_1-D_3. The diode voltages correspond to the respective LED string voltage drops: V_{D1} = 136 V, V_{D2} = 133 V, V_{D3} = 132 V. The current of the transistor Q_K increases with index K, while the maximum drain-to-source voltage Vds_K drops from transistor Q_1 to Q_3, which provides a basis for efficient transistor selection. In this simulation scenario, an implementation with electrolytic capacitors is considered, ensuring a continuous current supply to the LEDs. In this way, the current consumption of LED strings is easily estimated. However, electrolytic capacitors are not essential for the operation of the proposed driver. The current consumption of the LED strings exhibits a minor reduction as the index K increases from 1 to 2. Notably, the current consumption and, hence, power of the highest-indexed LED string, LED_3, are significantly lower than those of LED_1 and LED_2, which may be beneficial for optimization. As shown in Figure 3, as the inductor current reaches the upper threshold twice consecutively, an additional LED string is connected in series, leading to a current decrease.

Conversely, when the inductor current reaches the lower reference threshold twice in succession, one LED string is short-circuited, causing the current to increase. These transitions between operating stages take a finite amount of time, introducing input current distortion and reducing the power factor, as the average inductor current deviates from the ideal sinusoidal waveform. However, the power factor can be improved by reducing the inductor value, thereby decreasing transition time. Alternatively, decreasing the hysteresis band would bring the inductor current closer to the desired average value. Note that the Schottky diode D_1 conducts continuously throughout the input half-period, while diode D_2 conducts only during Stages(2) and (3), and diode D_3 conducts only during Stage(3). At high instantaneous input voltages, all three Schottky diodes conduct simultaneously, contributing to the overall conduction losses.

2.2. The second proposed boost LED driver

The distinctive feature of the second proposed driver, shown in Figure 1(b), is that it operates with two active stages and therefore utilizes only two Schottky diodes and the additional LED_0 string. The two active stages are controlled by two transistors, Q_1 and Q_2, one per stage. The presence of the LED_0 string introduces a skip mode. The skip mode of PWM regulation occurs at input line voltages $|Vin| \leq V_{LED0}$. The LED_0 string provides a voltage margin to make it possible to implement Schottky diodes for D_1 and D_2 by limiting their absolute reverse voltage. This voltage margin is ensured by the non-zero voltage V_{LED0} of the LED_0 string.

To evaluate the performance of this design, a computer model was developed using the same framework as for the first proposed driver. The model realizes power-factor correction through direct regulation of the inductor current in CCM, following the control approach described in section 2.1. The simulation setup, control strategy, and modeling assumptions remain identical to those of the first proposed driver, except for the reduced number of power switches and protective diodes.

The simulation model, shown in Figure 4, includes an AC input voltage source Vin, a diode bridge rectifier, the boost inductor L, a segmented LED load consisting of LED strings LED_0-LED_2, power transistors Q_1 and Q_2, and the same hysteresis-based current control circuit operating in CCM. As in the first model, the inductor current is regulated between upper and lower hysteresis thresholds using comparator-based control logic, while a DEMUX block governs transitions between operating stages. The control circuitry and DEMUX block are identical, without modification, to those used for the first proposed driver.

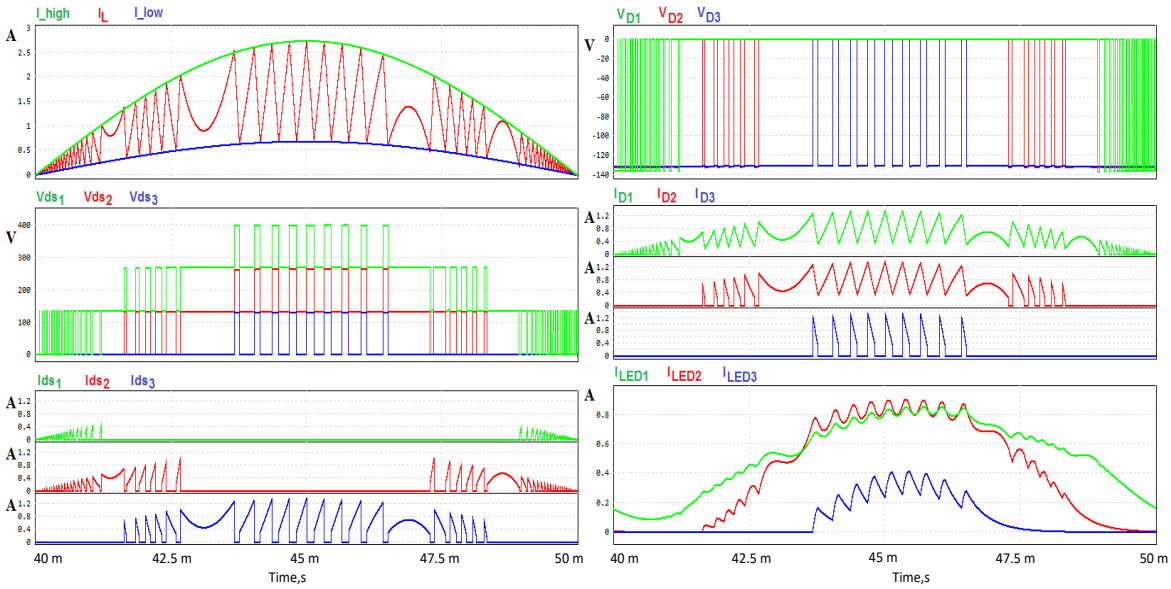

Figure 3. Simulation waveforms of the proposed LED driver. I_high ,I_low, I_L - comparators high/low values and inductor L current. Vds_1 , Vds_2 , Vds_3 - drain voltages on Q_1-Q_3 transistors. Ids_1 , Ids_2, Ids_3 - currents of Q_1-Q_3 transistors. V_{D1} , V_{D2} , V_{D3} - reverse voltages on diodes D_1-D_3. I_{D1} , I_{D2} , I_{D3} - currents of diodes D_1-D_3. I_{LED1} , I_{LED2} , I_{LED3} - currents of corresponding LED strings

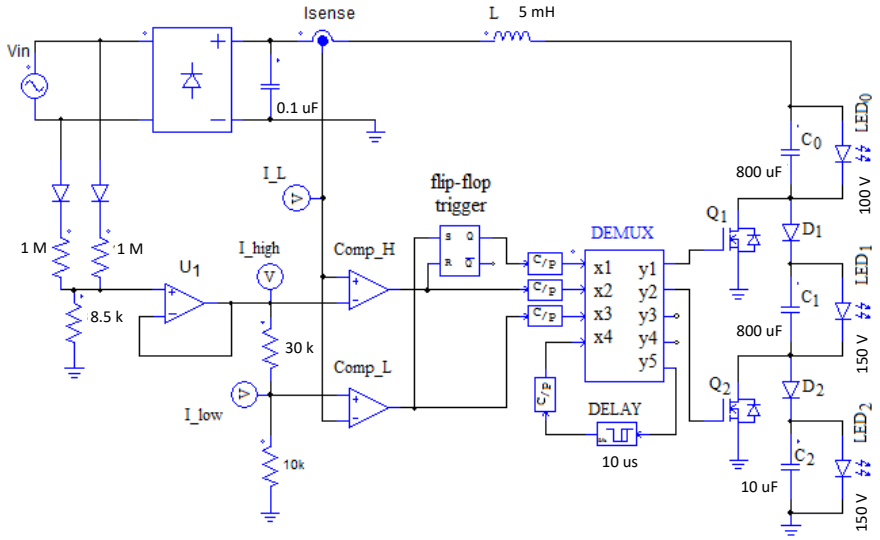

Figure 4. Computer simulation model of the second proposed boost LED driver

The input voltage is set to Vin = 230 Vrms with an input power of 136 W. For better visualization of the switching behavior, the boost inductor L is chosen as 5 mH, which reduces the switching frequency and makes the pulse switching traceable over the input voltage half-cycle. The voltage drops across the LED strings are set to V_{LED0}=100 V, V_{LED1}=150 V, and V_{LED2} = 150 V to correspond to experimental setup values.

Total voltage drop of LEDs is 400 V. Figure 5 presents the steady-state waveforms obtained from the computer modeling for a single half-period of the input voltage. The simulation shows the presence of skip mode in the PWM generation at input voltages |Vin| ≤ V_{LED0}. While skip mode conserves power, it negatively impacts power factor. Therefore, the value of V_{LED0} must be selected carefully to balance efficiency and power quality. The simulation results validate the feasibility of the proposed control method for the hybrid LED driver. The DEMUX block remains the same as for the model in Figure 2. The same DEMUX algorithm operates successfully despite variations in LED string voltage drops and LED load configurations.

The switching voltage amplitudes of two active transistor and protective diodes are reduced and equal the LED string voltages correspondingly. Note that the Schottky diode D_1 conducts during Stages(1) and (2), while diode D_2 conducts only during Stages(2). At high instantaneous input voltages, both Schottky diodes conduct simultaneously, contributing to the overall conduction losses.

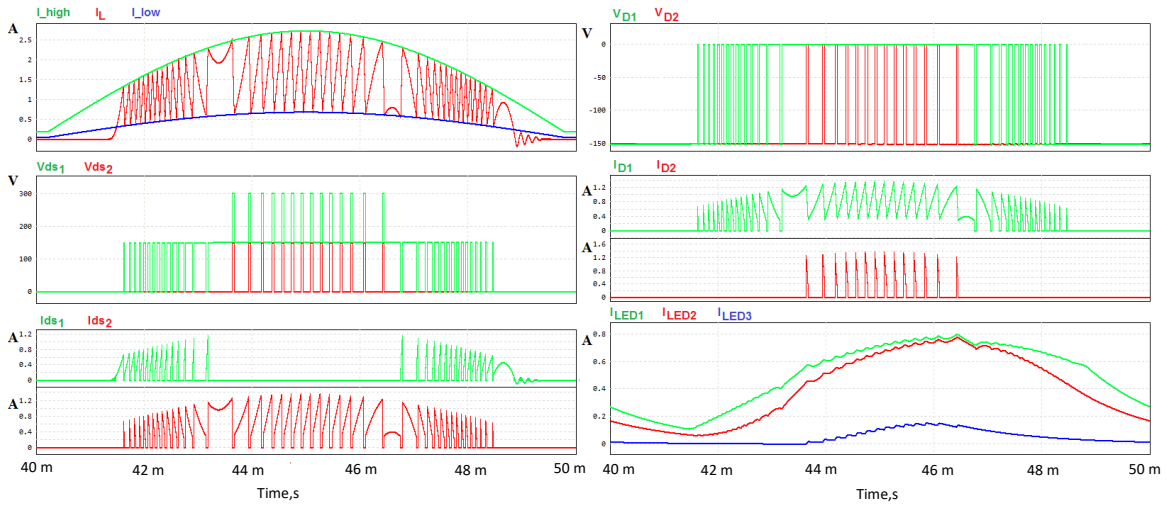

Figure 5. Simulation waveforms of the proposed LED driver. I_high ,I_low, I_L - comparators high/low values and inductor L current. Vds_1, Vds_2 - drain voltages on Q_1 and Q_2 transistors. Ids_1, Ids_2 - currents of Q_1 and Q_2 transistors. V_{D1} , V_{D2} - reverse voltages on diodes D_1 and D_2. I_{D1} , I_{D2} - currents of diodes D_1 and D_2. I_{LED0} , I_{LED1} , I_{LED2} - currents of corresponding LED strings

3. METHOD

3.1. Experimental set-up

Three laboratory samples with 200 W input power ratings were created to test the proposals: the sample of the first proposed driver, as shown in Figure 1(a); the sample of the second proposed driver, as shown in Figure 1(b); and one sample of the conventional boost driver. All samples incorporate power factor correction (PFC) and were assembled on a single printed circuit board to enable reliable comparison. Figure 6 illustrates the general electrical circuit of the printed circuit board for all test samples. The Line and Neutral terminals are to be connected to the AC mains source, which is rectified by the diode bridge Db_1. Common-mode chokes LF_1 and LF_2 are implemented at the input to suppress conducted electromagnetic interference generated by the LED driver during switching operation. The input circuitry of the board up to the main inductor L_1 is universal across all samples. The rectified input power is then processed by one of the three assembled driver configurations under test to supply the LED load with power factor correction (PFC). The characteristics of non-replaceable magnetic and passive components are shown in the diagram. Part numbers for semiconductors are shown in the diagram. Figure 7 specifies the output schematics of the sample drivers, with the power inductor L_1 parameters specified for each design. The transistor Q_{d1}, diode D_{d1}, and capacitor C_{d1} form the output of the conventional boost converter, see Figure 7(a). The transistors Q_1-Q_3, diodes D_1-D_3, and capacitors C_1-C_3 form the output of the proposed first LED driver, see Figure 7(b). The second proposed driver is obtained from the first by eliminating the transistor Q_1 and short-circuiting the diode D_1, as shown in Figure 7(c). Inductor L_1 is selected individually for each sample to account for differences in voltage ripple. LED_1, LED_2, and LED_3 strings shown in Figure 6 are the same output load and reconfigurable for each sample. For all samples, the rated input voltage range was selected as 150-270 Vac, and the rated input frequency range was 43-63 Hz.

The conventional boost driver was optimized for high efficiency given the input range 150-270 Vac. As a result of the optimization, the boost driver operates in the CrCM to benefit from zero current switching (ZCS) and QRS. Any standard CrCM controller providing power factor correction and QRS can be employed, as the choice of a specific controller does not affect the conclusions of this paper. The same controller approach is applied to the other two drivers for a fair comparison. Consequently, two input filter chokes, LF_1 and LF_2, were required, following the standard practice, to reduce current ripple in the conventional driver. Although the computer models employ hysteresis current control for generality, all experimental samples operate in CrCM mode as a special case to take advantage of ZCS and QRS. Implementation of CrCM mode is no problem for the developed control circuit and the proposed transition algorithm between operational stages. The control circuit remains universal across the samples, requiring no readjustments or additional tuning.

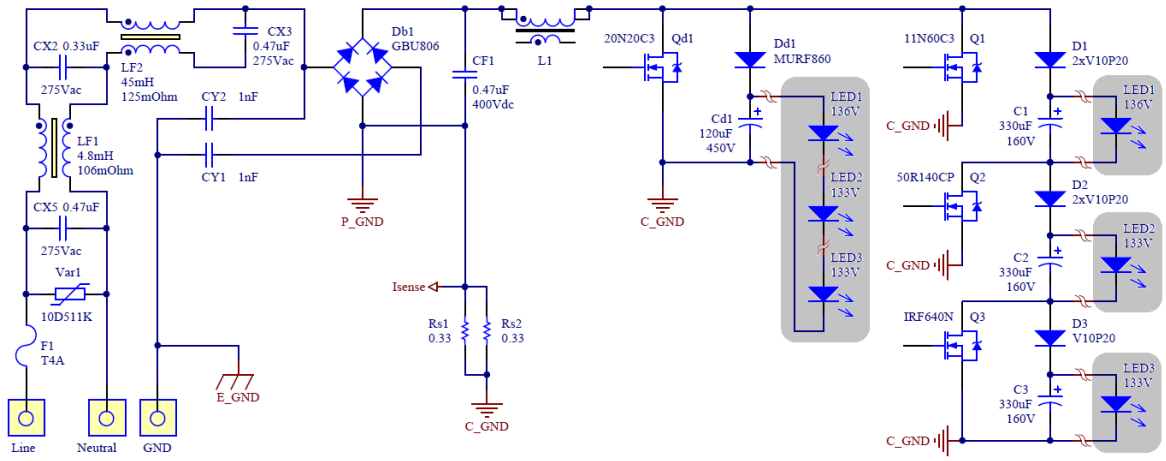

Figure 6. The electrical scheme of the experimental printed circuit board

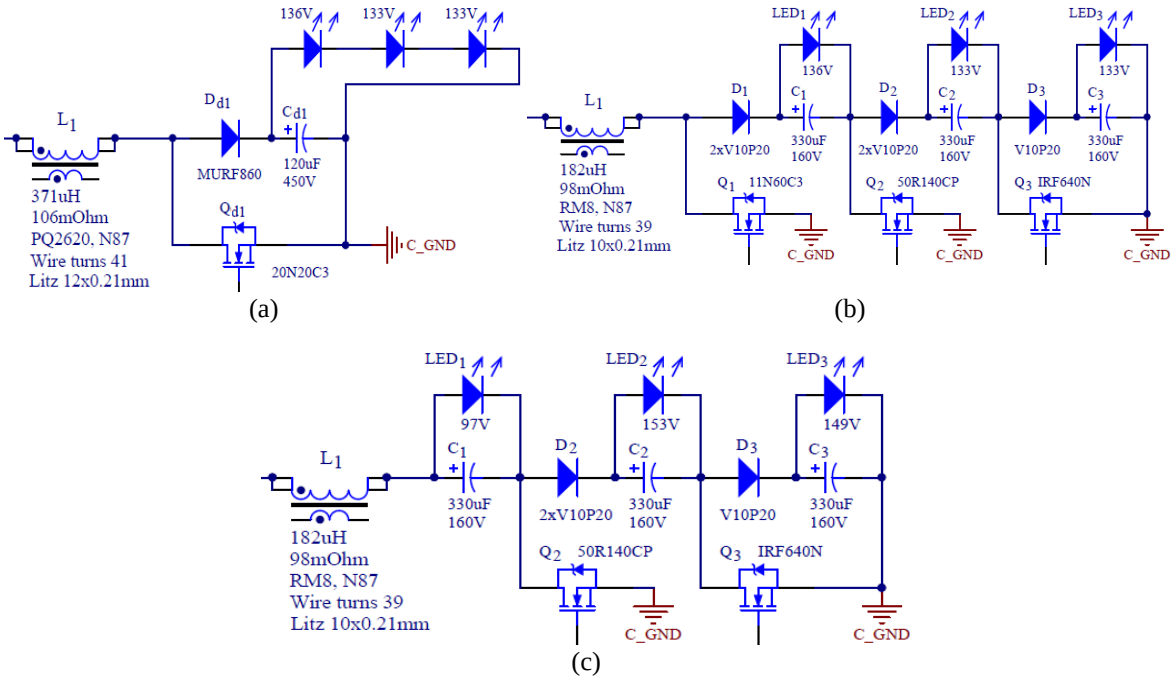

Figure 7. Electrical circuits of laboratory samples: (a) The output of the conventional LED boost driver; (b) The output of the first proposed LED driver; and (c) The output of the second proposed LED driver

The conventional driver employs an MURF860 diode as a power rectifier, while the proposed drivers utilize V10P20 Schottky diodes. These Schottky diodes, rated for 200 V, feature a compact TO-277A surface-mount package. Electrolytic capacitors C_1-C_3 were included solely to improve efficiency measurements by minimizing voltage and current ripple in the LED strings. The inductance of L_1 was selected individually for each sample to ensure an equivalent switching frequency pattern, see Figure 8.

For the conventional driver, L_1 was set to 371 µH with a PQ2620 core. In contrast, the proposed drivers required a significantly smaller inductor, with L_1 reduced to 182 µH and utilizing an RM8 core. Experimental measurements were conducted for each sample at a 50 Hz input line frequency and for line voltages of 160 Vac, 230 Vac, and 270 Vac.

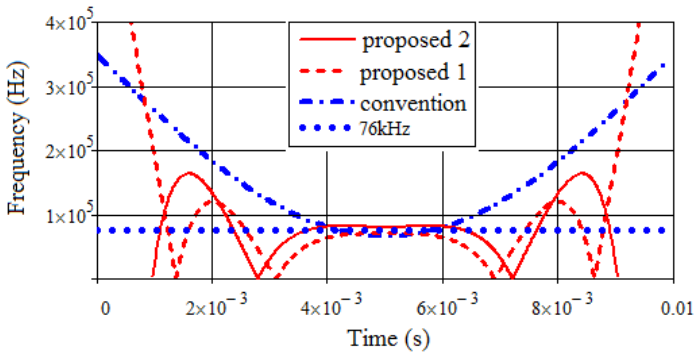

Figure 8. Calculated instantaneous PWM frequency of samples within half of the line period: dash dot line - conventional driver, dashed line - first proposed driver, solid line - second proposed driver, and dotted line - 76 kHz

In the proposed LED driver samples, quasi-resonant switching and dynamic LED-segment reconfiguration synchronized with the input voltage were achieved as follows. The same standard critical conduction mode PWM controller with QRS as that used in the conventional driver sample was implemented. In typical controllers, QRS can be realized using different approaches, such as introducing a time delay after the inductor current reaches zero or detecting the voltage valley via the auxiliary winding of the inductor. The specific choice of the controller is not critical to the main results of this paper; however, it is essential that the same controller be used for all samples under test in order to employ an identical QR switching principle, thereby ensuring consistent test conditions and a reliable performance comparison. Within the controller, the PWM signal was generated by a conventional analog circuit comprising input-voltage and inductor-current sensing amplifiers, hysteresis comparators, and a flip-flop trigger. The resulting PWM signal was distributed to the MOSFET gate drivers controlling the stage power transistors. Stage selection and LED string reconfiguration were handled by a low-cost microcontroller implementing a DEMUX function, as described in subsection 2.1, which enables or disables the corresponding MOSFET gate drivers. The microcontroller operated exclusively as a slow supervisory unit at the mains-frequency time scale and did not generate PWM signals, execute fast control loops, or perform signal conditioning. Consequently, the internal implementation of the supervisory logic does not influence the operating principle, steady-state behavior, or the experimental results reported in this study.

The experimental arrangement is illustrated in Figure 9. The driver under test was powered by a programmable AC mains source (Chroma 61502) and connected to output LED strings. All driver topologies were implemented on a single printed circuit board to ensure identical electrical layout, input filtering, thermal conditions, and measurement environment, thereby enabling a fair and repeatable comparison. During testing, only one driver on the test board was energized at a time, while the remaining drivers were electrically disabled.

Input electrical quantities, including voltage, current, power factor, and harmonic distortion, were measured using a WT310E digital power analyzer with a specified accuracy of 0.1%. Harmonic analysis was performed up to the 40th harmonic order. Voltages across individual output LED strings were measured using Fluke 289/FVF digital multimeters with a specified DC voltage accuracy of 0.025%. LED string currents were obtained by Fluke 289/FVF multimeters measuring voltage drops across precision RX-70 current-sensing resistors (0.1 Ω, 0.01% tolerance, 1 W rating) connected in series with each LED channel. The true-RMS Fluke 289 multimeters provide galvanic isolation and accurate measurement of true DC components in floating differential potentials across the LED load segments and resistive current sensors. Experimental measurements were conducted at a fixed mains frequency of 50 Hz and input voltages of 160 Vac,

230 Vac, and 270 Vac, over an output power range from 20 W to 220 W. All experiments were performed under natural air convection at an ambient temperature of approximately 25 °C. Device temperatures were monitored using an infrared camera and thermocouples to verify steady-state thermal conditions. Prior to data acquisition, the system was allowed to reach thermal equilibrium, which was confirmed by stable electrical readings.

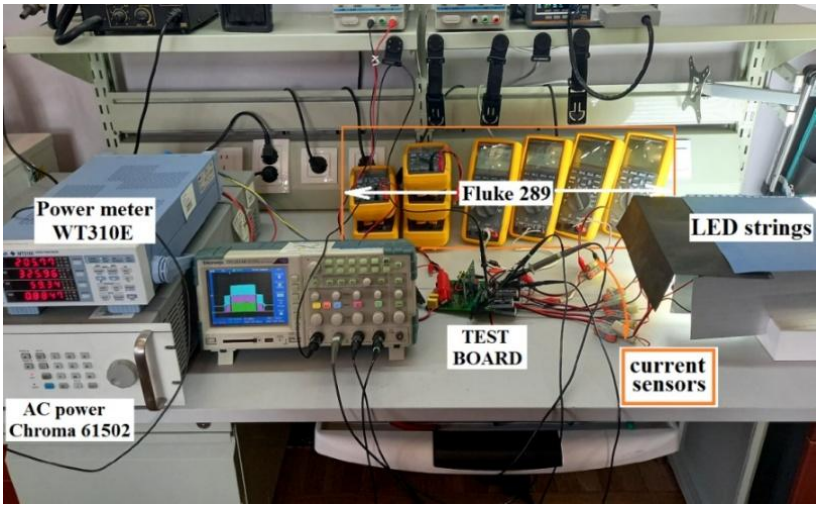

Figure 9. The experimental setup for the conventional, first, and second proposed drivers

3.2. Experimental results of the first proposed boost LED driver

Figure 10 presents waveforms of the first proposed LED driver, with an output as shown in Figure 7(b), at 200 W input power and 230 V input voltage. Waveforms of transistors Q_1-Q_3 and the inductor current closely align with the simulated results in Figure 3, except for the switching frequency and the hysteresis value. The control circuit in the proposed driver provides ZCS and QRS for each active transistor from Q_1-Q_3 in the corresponding active stage (K). Figure 11 demonstrates that the transistors turn on resonantly at the minimum drain voltage, minimizing dynamic losses.

Specifically, Figures 11(a) and 11(e) illustrate the switching process of the transistor Q_1 at Stage(1). Figures 11(b) and 11(d) illustrate the switching process of the transistor Q_2 at Stage(2), while Figure 11(c) presents the switching-on process of the transistor Q_3 at Stage(3). Finally, Figure 12 compares the efficiencies of the proposed driver with an output as in Figure 7(b) and the conventional boost driver with an output shown in Figure 7(a). At high loads, both drivers exhibit identical efficiency.

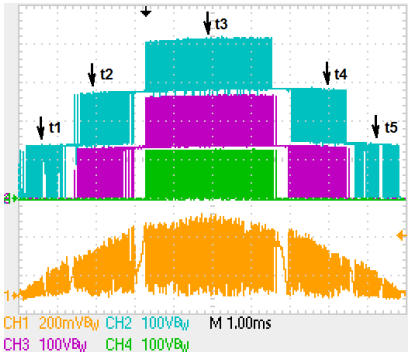

Figure 10. Experimental voltage and current waveforms of the first proposed LED driver are shown in Figure 7(b), illustrating the stage-wise operation of the converter: CH1 - inductor current, data from I_sense; CH2 - voltage on the transistor Q_1; CH3 - voltage on the transistor Q_2; CH4 - voltage on the transistor Q_3

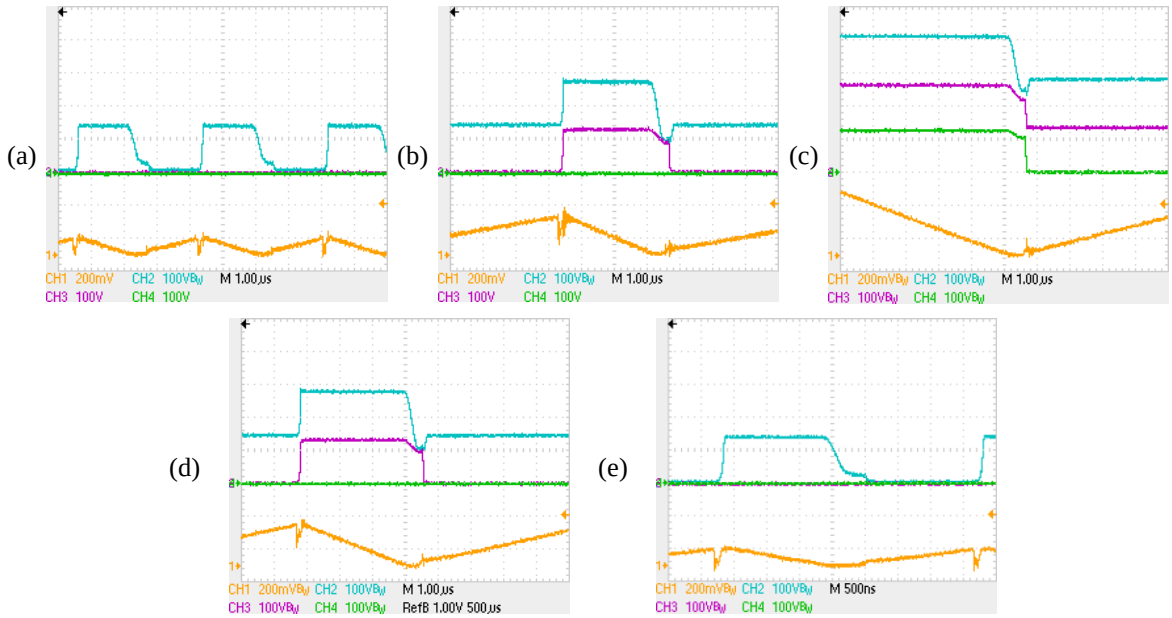

Figure 11. Experimental waveforms of the first proposed LED driver at the marked time moments shown in Figure 10, illustrating ZCS and QRS of stage transistors: (a) at the time moment t1; (b) at the time moment t2; (c) at the time moment t3; (d) at the time moment t4; (f) at the time moment t5

However, at light loads, the proposed driver demonstrates higher efficiency, indicating reduced dynamic losses, as expected. At high loads, the benefits of reduced switching losses are offset by the conduction losses in the three series-connected Schottky diodes. Figure 13 presents the power factor measurements, showing that the power factor of the proposed driver is affected by input current distortion during stage transitions. The measured power factor is 0.963, with a total harmonic distortion (THD) of 12.6% at an input voltage of 230 Vac and an input power of 200 W.

3.3. Experimental results of the second proposed boost LED driver

Figure 14 presents the waveforms of the second proposed LED driver with an output shown in Figure 7(c), operating at an input power of 195 W and an input voltage of 230 Vac. The waveforms of transistors Q_2, Q_3, and the inductor current closely align with the simulated results in Figure 5, except for differences in switching frequency and the hysteresis value. The control circuit in the proposed driver successfully implements ZCS and QRS for both transistors Q_2 and Q_3, as long as the transistor is active in the corresponding Stage(K).

Table 1 presents the steady-state temperatures of the driver components measured at an input power of 200 W, an input voltage of 230 V, and an ambient temperature of 25 °C. The driver efficiency at this operating point is 98.5%, corresponding to a total power loss of approximately 3 W. Table 1 also lists the estimated power losses of individual components, derived from measured temperature rise, equivalent resistance measurements, and calculated loss values.

Table 2 presents the measured harmonic content of the driver's input current compared with the requirements of IEC 61000-3-2 Class C for lighting equipment. Figure 15(a) presents the power factor measurements. The power factor of the proposed driver is worsened by skip mode and by input current distortion during the transition process Stage(1)↔Stage(2). The measured power factor is 0.958, THD is 15.6% at Vin = 230 Vac and Pin = 195 W.

Finally, Figure 15(b) compares the efficiencies of the proposed and conventional boost drivers. The second proposed driver demonstrates significantly higher efficiency at both light and high loads owing to lower dynamic and conduction losses. This improvement is attributed to the reduced voltage drop across the two Schottky diodes compared to the MURF860 rectifier used in the conventional driver. At loads below 80 W, the forward voltage drop across the LED load decreases. Therefore, at a high input voltage of 270 Vac, the peak rectified voltage exceeds the LED load voltage, which worsens the power factor. Since the current through the LED load becomes unregulated, efficiency measurements at 270 Vac and loads below 80 W were not performed for either the proposed or the conventional driver (see Figures 13 and 15).

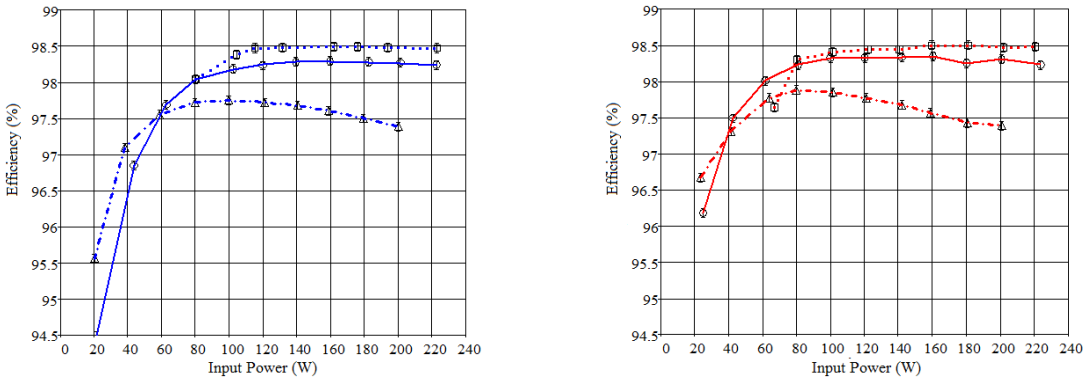

Figure 12. Measured efficiency of the first proposed LED driver in comparison with a conventional driver, indicating efficiency improvement of the proposed design, square dots - at 270 Vac input, round dots - at 230 Vac input, triangle dots - at 160 Vac input: (a) the conventional driver and (b) the first proposed driver

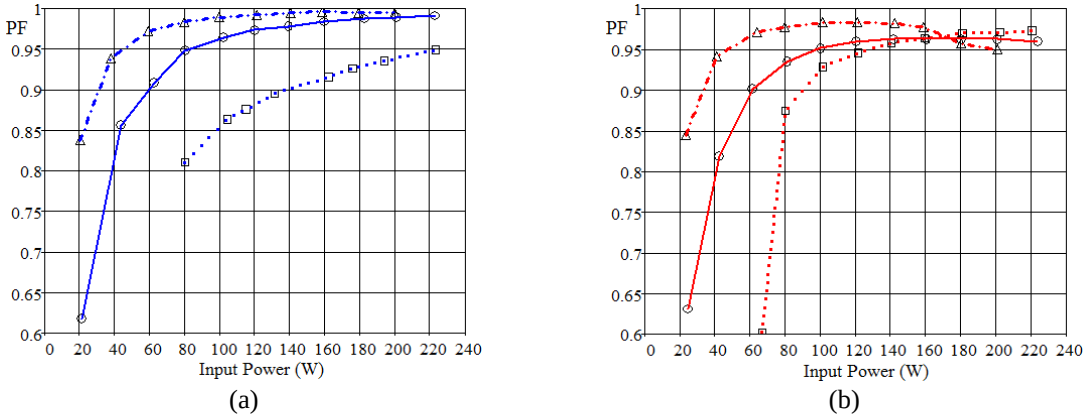

Figure 13. Measured power factor of the first proposed LED driver in comparison with a conventional driver, square dots - at 270 Vac input, round dots - at 230 Vac input, triangle dots - at 160 Vac input: (a) the conventional driver and (b) the first proposed driver

Figure 14. Experimental waveforms of the second proposed LED driver shown in Figure 7(c), illustrating two-stage operation of the driver: CH1 - inductor current, data from I_sense; CH3 - voltage on the transistor Q_2; CH4 - voltage on the transistor Q_2

Table 1. Component temperatures and corresponding power losses, ambient temperature T_{amb} = 25 °C

Parameter	Input filters	Diode bridge	Inductor L_1	MOSFET Q_2	Diode D_2	MOSFET Q_3	Diode D_3	Current sensor	Output caps	Control	PCB
Temp, °C	-	70	37	31	54	39	33	-	-	-	-
Power loss, W	0.28	1.2	0.21	0.1	0.39	0.2	0.11	0.17	0.13	0.09	0.1

Table 2. Measured harmonics of the driver compared to the IEC-61000-2-3, Vin = 230 Vac and Pin = 195 W

Harmonic, No.	3	5	7	9	11	13	15	17	19	21	23	25	27-39
Measured	7,5%	8,1%	4,7%	3,0%	3,4%	0,9%	1,5%	3,1%	0,6%	3,3%	1,3%	2,8%	<3%
IEC-61000-3-2, class C	29%	10%	7,0%	5,0%	3,0%	3,0%	3,0%	3,0%	3,0%	3,0%	3,0%	3,0%	3,0%
Status	pass	pass	pass	pass	fail	pass	pass	fail	pass	fail	pass	pass	pass

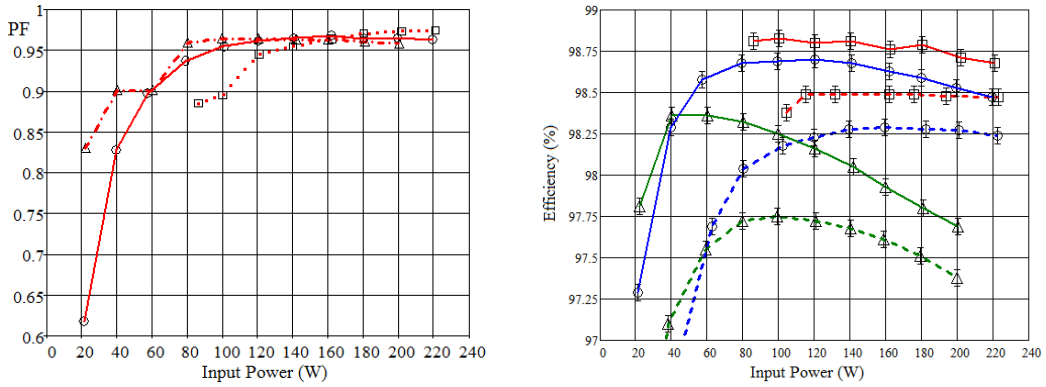

(a) (b)

Figure 15. Experimental measurements of the second proposed LED driver, illustrating superior efficiency of the proposed design, square dots - at 270 Vac input, round dots - at 230 Vac input, triangle dots - at 160 Vac input, dashed lines - the conventional driver; solid lines - the second proposed driver: (a) power factor and (b) efficiency

4. RESULTS AND DISCUSSION

The developed control circuit has proven to be universal for the tested samples, operating automatically without requiring additional tuning. It is confirmed that the proposed transition algorithm remains resistant to input voltage noise. The proposed LED drivers are triac-dimmable, since they operate based on the presence of instantaneous input voltage. It is possible to integrate digital, PWM, or analog dimming control.

The proposed drivers can operate over a wide input voltage range of 90-270 Vac. For the first proposed driver, at low input voltages Vin < 110 Vac, only transistor Q_1 is active, lighting LED_1. Therefore, the driver must either be derated or Q_1, together with LED_1, must be rated for 200 W. For the second proposed driver, the power factor will be unacceptable unless the LED load is redesigned for low input voltage.

The article examines two drivers to show how the number of Schottky diodes greatly affects efficiency under otherwise identical conditions, PWM frequency pattern, and the inductor. Both LED drivers achieve higher efficiency than the conventional boost PFC driver, as shown in Figures 12 and 15(b). The component temperature rise remains moderate under natural convection, indicating low semiconductor stress and good thermal robustness. Due to low pulse voltage across the main inductor and power switches, the inductor size and switching losses in power components are reduced. The increased conduction losses in diodes are mitigated by the implementation of a small number of Schottky diodes. The high efficiency of the second proposed driver comes at the expense of a reduced power factor. At 230 Vac, the measured efficiency reaches 98.7% at half load, while at full load the total power loss is approximately 3 W. Harmonic analysis demonstrates compliance with IEC 61000-3-2 Class C limits for most harmonic components, with only minor exceedances near the specified limits, indicating that the power factor and harmonic performance can be further optimized through control and parameter refinement.

The proposed drivers have undergone first-stage optimization but still offer room for further refinement. For instance, in the first proposed driver (see Figure 8(b)), Schottky diodes rated at 150 V could be used. The analysis of the second proposed driver highlights the need for careful skip mode time adjustment, as it presents a trade-off between power factor and the voltage ratings of Schottky rectifiers. The skip-mode operation preserves power efficiency as long as the RMS current values remain moderate, by skipping ineffective low-power conversion. Moreover, the higher the voltage V_{LED0}, the smaller the values that can be selected for V_{LED1} and V_{LED2}, resulting in correspondingly lower reverse voltages across diodes D_1 and D_2. In this case, Schottky diodes with a lower forward voltage drop can be used, thereby improving the overall efficiency of the driver. But skip-mode negatively affects the power factor, as shown in Figure 5. In the second proposed driver, the harmonic distortions are very close to the standard compliance limits. As

shown in Table 2, some harmonics slightly exceed the specified levels. Therefore, the power factor can be improved by reducing the voltage V_{LED0} and thereby shortening the skip-mode duration.

The diodes used in the second driver are rated for 200 V. Accordingly, the voltages of the LED loads LED_1 and LED_2 can be selected higher so that the voltage across LED_0 is lower, thereby reducing skip-mode operation and improving the power factor. For example, by selecting relatively high string voltages V_{D1} and V_{D2} of approximately 180 V each in Figure 1 (b), while leaving a 20 V margin for the 200 V diodes D_1 and D_2, the voltage of the LED_0 string can be set to V_{LED0} = 400 V-180 V-180 V = 40 V. In this configuration, the power factor is significantly improved, while the overall efficiency may not necessarily decrease, since both the RMS input current and the effective currents in the driver circuits are reduced.

The input current distortions are also caused by transient processes Stage(K)↔Stage(K+1). To reduce these distortions, different strategies can be investigated in the future, including some subtle adaptive methods, the essence of which will be to eliminate zero-frequency points of the PWM in the control, see Figure 9. Optimizing the ON/OFF time ratios of transistor Q_K could potentially identify the correct moments for stage transitions, thereby replacing the criterion based on the double-hitting of current references. Possibly, imposing a maximum ON and/or OFF time limit on the transistors could serve the same purpose, helping to restrict the minimum switching frequency. Another solution could be a temporary transition to continuous conduction mode (CCM), along with narrowing the current hysteresis band closer to the required average value, for the duration of the Stage(K) ↔Stage(K+1) transitions. Another option is to reduce the inductance, thereby shortening the transient time and, consequently, decreasing its impact on current distortion. This would increase the switching frequency, but the impact on efficiency may not be substantial if the drivers operate in CrCM with QRS. However, if these measures are not sufficient, transitioning to (CCM) with a reduced current hysteresis band should be considered. Optimizing the system remains a complex challenge due to the numerous interdependent parameters.

The proposed drivers can operate without electrolytic capacitors in parallel with the LED strings. In the computer simulation, electrolytic capacitors were included in the circuit only for the analysis of load currents. In the experiments, electrolytic capacitors were introduced to improve the accuracy of voltage and current consumption measurements of LED strings and to calculate the efficiency with high accuracy. The LED configuration algorithm operates at a low frequency, is highly practical, realizable, and potentially low-cost. These characteristics make it possible to develop a universal control chip. Further integration of the power semiconductor devices is feasible due to the low losses. As can be seen from Table 1, the total power losses associated with the two active MOSFETs and the control circuit amount to approximately 0.4 W. Such low losses facilitate monolithic integration, which is expected to reduce cost, further improve reliability, and relax design constraints commonly encountered in large-scale outdoor and industrial lighting installations. In the future, the integration of protective Schottky diodes may also be implemented to further reduce circuit complexity and cost. The diodes would contribute only about 0.5 W of additional power loss within the chip. From an application perspective, the proposed driver is particularly relevant for high-power LED systems such as street lighting, industrial luminaires, and infrastructure lighting, where long operating lifetimes, high efficiency, and minimal maintenance are critical.

5. CONCLUSION

This paper has investigated the proposed boost LED drivers aimed at high-power lighting applications. The drivers significantly reduce switching losses by lowering high-frequency pulsed voltages through dynamic LED string reconfiguration and quasi-resonant zero-current switching, while maintaining low conduction losses by employing a limited number of Schottky protection diodes. Simulation and experimental results were presented to validate these claims. Experimental prototypes rated for 200 W were developed, and their performance was compared against a high-efficiency conventional boost driver. The proposed drivers demonstrated superior efficiency compared to the conventional design. One prototype achieved an efficiency of up to 98.7% at 120 W input power. The study also identified limitations and potential areas for improvement. The apparent complexity of the proposed drivers could be mitigated by integrating the control and power stages into a single chip. To enhance efficiency, power factor, reliability, and cost-effectiveness, future work will focus on optimizing LED string segmentation for different power levels, improving the trade-off between efficiency and power factor, optimizing the PWM switching strategy, and the power inductor.

ACKNOWLEDGMENTS

The authors acknowledge Kazakh-British Technical University for providing research facilities and institutional support. The authors also acknowledge the Science and Innovation Department of the University for its organizational support.

FUNDING INFORMATION

The work was funded by the Science Committee of the Ministry of Education and Science of the Republic of Kazakhstan under project AP No.19678370, titled "Research and Development of a hybrid LED driver".

AUTHOR CONTRIBUTIONS STATEMENT

This journal uses the Contributor Roles Taxonomy (CRediT) to recognize individual author contributions, reduce authorship disputes, and facilitate collaboration.

Name of Author	C	M	So	Va	Fo	I	R	D	O	E	Vi	Su	P	Fu
Dzhunusbekov Erlan	✓	✓	✓	✓	✓	✓	✓	✓	✓	✓	✓	✓	✓	✓
Orazbayev Sagi	✓	✓	✓	✓	✓	✓	✓	✓	✓	✓	✓	✓	✓	✓

C : **C**onceptualization
M : **M**ethodology
So : **So**ftware
Va : **Va**lidation
Fo : **Fo**rmal analysis
I : **I**nvestigation
R : **R**esources
D : **D**ata Curation
O : Writing - **O**riginal Draft
E : Writing - Review & **E**diting
Vi : **Vi**sualization
Su : **Su**pervision
P : **P**roject administration
Fu : **Fu**nding acquisition

CONFLICT OF INTEREST STATEMENT

Authors state no conflict of interest.

DATA AVAILABILITY

All data supporting the findings of this study are available within the manuscript. No additional data are available.

REFERENCES

[1] H. Zhang, "A viable nontesting method to predict the lifetime of LED drivers," *IEEE Journal of Emerging and Selected Topics in Power Electronics*, vol. 6, no. 3, pp. 1246–1251, Sep. 2018, doi: 10.1109/JESTPE.2018.2826364.

[2] M. K. Barwar, L. K. Sahu, and P. Bhatnagar, "Reliability analysis of PFC multilevel rectifier based LED driver circuit," in *2022 Second International Conference on Power, Control and Computing Technologies (ICPC2T)*, Mar. 2022, pp. 1–5. doi: 10.1109/ICPC2T53885.2022.9776846.

[3] M. Demir, A. B. Yildiz, and T. Agir, "Observation of the effects of electrostatic discharge and lightning surge on the reliability of a LED circuit driven by half-bridge converter," in *2018 International Symposium on Power Electronics, Electrical Drives, Automation and Motion (SPEEDAM)*, Jun. 2018, pp. 1073–1078. doi: 10.1109/SPEEDAM.2018.8445297.

[4] P. Watte, G. van Hees, R. Engelen, W. . van Driel, and T. Chen, "Reliability of electronic drivers: an industrial approach," in *2021 18th China International Forum on Solid State Lighting & 2021 7th International Forum on Wide Bandgap Semiconductors (SSLChina: IFWS)*, Dec. 2021, pp. 246–249. doi: 10.1109/SSLChinaIFWS54608.2021.9675170.

[5] B. Liu, J. Qi, X. Yin, and Y. Sun, "Consistency and degradation of electrochemical double layer capacitors under calendar ageing," in *2020 Global Reliability and Prognostics and Health Management (PHM-Shanghai)*, Oct. 2020, pp. 1–5. doi: 10.1109/PHM-Shanghai49105.2020.9280955.

[6] E. J. Dzhunusbekov and S. A. Orazbayev, "Electrolytic capacitor life time calculation under varying operating conditions," *Journal of Vibroengineering*, vol. 22, no. 3, pp. 721–734, May 2020, doi: 10.21595/jve.2019.20733.

[7] OSRAM, "Reliability and lifetime of LEDs application," 2022. [Online]. Available: https://look.ams-osram.com/m/738267cd95c87869/original/Reliability-and-lifetime-of-LEDs.pdf

[8] K. Awad, O. Abdel-Rahim, M. A. Gaafar, and M. Orabi, "Design methodology of an electrolytic capacitorless LED driver using SEPIC PFC converter," in *2023 IEEE Conference on Power Electronics and Renewable Energy (CPERE)*, Feb. 2023, pp. 1–6. doi: 10.1109/CPERE56564.2023.10119530.

[9] D. Salazar-Perez, M. Ponce-Silva, J. M. Alonso, J. A. Aqui-Tapia, and C. Cortes-Garcia, "A novel high-power-factor electrolytic-capacitorless LED driver based on ripple port," *IEEE Journal of Emerging and Selected Topics in Power Electronics*, vol. 9, no. 5, pp. 6248–6258, Oct. 2021, doi: 10.1109/JESTPE.2021.3066145.

[10] Y. Qu and L. Qiu, "I 2 V 2 average current control for modular LED drivers," *IEEE Transactions on Power Electronics*, vol. 36, no. 1, pp. 78–82, Jan. 2021, doi: 10.1109/TPEL.2020.3005571.

[11] G. Z. Abdelmessih, J. M. Alonso, N. da S. Spode, and M. A. D. Costa, "Electrolytic-capacitor-less off-line LED driver based on integrated parallel buck-boost and boost converter," in *2020 IEEE Industry Applications Society Annual Meeting*, Oct. 2020, pp. 1–7. doi: 10.1109/IAS44978.2020.9334804.

[12] L. Cao, Y. Zhu, and H. Wu, "A new electrolytic capacitor-less LED driver with coupled-inductor," in *2020 IEEE Applied Power Electronics Conference and Exposition (APEC)*, Mar. 2020, pp. 1537–1543. doi: 10.1109/APEC39645.2020.9124527.

[13] G. Z. G. Abdelmessih, J. M. Alonso, N. Spode, and M. A. Dalla Costa, "High-efficient electrolytic-capacitor-less off-line LED driver with reduced power processing," *IEEE Transactions on Power Electronics*, vol. 37, no. 2, pp. 1804–1815, 2021, doi: 10.1109/TPEL.2021.3108137.

[14] M. Esteki, D. Darvishrahimabadi, M. Shahabbasi, and S. A. Khajehoddin, "An electrolytic-capacitor-less PFC LED driver with low DC-bus voltage stress for high power streetlighting applications," *IEEE Transactions on Power Electronics*, vol. 38, no. 5, pp. 6294–6310, May 2023, doi: 10.1109/TPEL.2023.3236013.
[15] C. Le, D. L. Gerber, M. Kline, S. R. Sanders, and P. R. Kinget, "Reconfigurable hybrid-switched-capacitor-resonant LED driver for multiple mains voltages," *IEEE Journal of Emerging and Selected Topics in Power Electronics*, vol. 6, no. 4, pp. 1871–1883, Dec. 2018, doi: 10.1109/JESTPE.2018.2859408.
[16] FAIRCHILD, "Guidance of using LED direct-AC driver design tool for FL77904/FL77944/FL77905," 2016.
[17] H. Gao *et al.*, "An electrolytic-capacitorless and inductorless AC direct LED driver with power compensation," in *2015 IEEE 2nd International Future Energy Electronics Conference (IFEEC)*, Nov. 2015, pp. 1–5. doi: 10.1109/IFEEC.2015.7361491.
[18] K. I. Hwu and W. C. Tu, "Controllable and dimmable AC LED driver based on FPGA to achieve high PF and low THD," *IEEE Transactions on Industrial Informatics*, vol. 9, no. 3, pp. 1330–1342, Aug. 2013, doi: 10.1109/TII.2012.2226042.
[19] H.-H. Chou, "Design and implementation of the linear LED driver," *IEEE Transactions on Circuits and Systems II: Express Briefs*, vol. 70, no. 3, pp. 1059–1063, Mar. 2023, doi: 10.1109/TCSII.2022.3219226.
[20] H. Zhang, "Developing highly reliable LED luminaires for high temperature applications using AC-direct driving LED technology," in *2018 IEEE Applied Power Electronics Conference and Exposition (APEC)*, Mar. 2018, pp. 3466–3470. doi: 10.1109/APEC.2018.8341602.
[21] S.-F. Wang, C.-M. Kung, Y.-C. Yeh, C.-R. Lee, and W.-T. Tsai, "Ultra-low percentage flicker high-efficiency direct AC LED driver using constant power technology," *IEEE Access*, vol. 11, pp. 97400–97407, 2023, doi: 10.1109/ACCESS.2023.3308197.
[22] L. Li, Y. Gao, and P. K. T. Mok, "A multiple-string hybrid LED driver with 97% power efficiency and 0.996 power factor," in *2016 IEEE Symposium on VLSI Technology*, Jun. 2016, pp. 1–2. doi: 10.1109/VLSIT.2016.7573396.
[23] Y. Gao, L. Li, K.-H. Chong, and P. K. T. Mok, "A hybrid LED driver with improved efficiency," *IEEE Journal of Solid-State Circuits*, vol. 55, no. 8, pp. 2129–2139, Aug. 2020, doi: 10.1109/JSSC.2020.2987730.
[24] K.-H. Chong, Y. Gao, and P. K. T. Mok, "A customized AC hybrid LED driver with flicker reduction for high nominal range applications," *IEEE Transactions on Circuits and Systems II: Express Briefs*, vol. 68, no. 5, pp. 1635–1639, May 2021, doi: 10.1109/TCSII.2021.3066416.
[25] O. Sagi and D. Erlan, "A new hybrid LED driver," *International Journal of Power Electronics and Drive Systems (IJPEDS)*, vol. 15, no. 4, p. 2367, Dec. 2024, doi: 10.11591/ijpeds.v15.i4.pp2367-2375.

BIOGRAPHIES OF AUTHORS

Dzhunusbekov Erlan is an associate professor and lecturer at the School of Materials Science and Green Technologies of the Kazakh-British Technical University, where he also serves as the Principal Investigator of the University's Electronics Laboratory. He received a Master's degree in Solid-State Physics from the National Research Nuclear University (MEPhI), Russia. Previously, he worked as a Lead Engineer at the Moscow Aviation Institute (National Research University) in the field of power electronics and as a Principal Engineer in the Advanced Power Team at Samsung Electro-Mechanics (South Korea). He conducts research and development in the areas of power electronics and robotics. He can be contacted at email: erlan555dj@yahoo.com.

Orazbayev Sagi holds a Ph.D. degree and serves as an Associate Professor. He graduated from the Faculty of Physics at Al-Farabi Kazakh National University, specializing in Materials Science and Technology of New Materials. He previously worked as a Lead Engineer in the Engineering Laboratory of the same university. His current research focuses on the investigation of advanced materials, improvement of light radiation energy efficiency, and the development of related technologies. He is the author of more than 90 scientific publications. In 2013, 2015, and 2018, he completed research internships at the GREMI Laboratory, Polytechnic University of Orléans (Orléans, France). He has led two nationally funded research projects in Kazakhstan and served as a responsible executor for 12 projects supported by national grants and program-targeted funding, as well as a commercialization project funded by the Science Foundation during 2017-2020. In recognition of his scientific contributions, he has received state awards and scholarships for young scientists. He can be contacted at email: sagi.orazbayev@gmail.com.